Annales Geophysicae, 23, 1723–1733, 2005
SRef-ID: 1432-0576/ag/2005-23-1723

Annales Geophysicae

The spherical segmented Langmuir probe in a flowing thermal plasma: numerical model of the current collection

E. Séran[1], **J.-J. Berthelier**[1], **F. Z. Saouri**[1], **and J.-P. Lebreton**[2]

[1]CETP, 4 Avenue de Neptune, 94100 Saint-Maur, France
[2]ESA/ESTEC, Postbus 299, NL-2200 AG Noordwijk ZH, The Netherlands

Received: 30 October 2004 – Revised: 22 February 2005 – Accepted: 14 April 2005 – Published: 28 July 2005

Abstract. The segmented Langmuir probe (SLP) has been recently proposed by one of the authors (Lebreton, 2002) as an instrument to derive the bulk velocity of terrestrial or planetary plasmas, in addition to the electron density and temperature that are routinely measured by Langmuir probes. It is part of the scientific payload on the DEMETER microsatellite developed by CNES. The basic concept of this probe is to measure the current distribution over the surface using independent collectors under the form of small spherical caps and to use the angular anisotropy of these currents to obtain the plasma bulk velocity in the probe reference frame. In order to determine the SLP capabilities, we have developed a numerical PIC (Particles In Cell) model which provides a tool to compute the distribution of the current collected by a spherical probe. Our model is based on the simultaneous determination of the charge densities in the probe sheath and on the probe surface, from which the potential distribution in the sheath region can be obtained. This method is well adapted to the SLP problem and has some advantages since it provides a natural control of the charge neutrality inside the simulation box, allows independent mesh sizes in the sheath and on the probe surface, and can be applied to complex surfaces. We present in this paper initial results obtained for plasma conditions corresponding to a Debye length equal to the probe radius. These plasma conditions are observed along the Demeter orbit. The model results are found to be in very good agreement with those published by Laframboise (1966) for a spherical probe in a thermal non-flowing plasma. This demonstrates the adequacy of the computation method and of the adjustable numerical parameters (size of the numerical box and mesh, time step, number of macro-particles, etc.) for the considered plasma-probe configuration. We also present the results obtained in the case of plasma flowing with mesothermal conditions reproducing the case of measurements onboard a low altitude spacecraft. Finally, we briefly discuss the capabilities of the SLP to deduce the plasma bulk velocity under similar conditions and present the first onboard measurements.

Keywords. Ionosphere (Modeling and forecasting; Instruments and techniques)

Correspondence to: E. Séran
(seran@cetp.ipsl.fr)

1 Introduction

The interaction between a flowing plasma and a charged body is a long-standing problem which has numerous practical applications, such as spacecraft charging or in-depth understanding of the operation of low energy plasma sensors (see, for example, Al'pert, 1974; Hastings and Garrett, 1996; Swift and Schwar, 1970). Spacecraft charging controls the sheath structure and then the distribution function of particles that are measured on board the spacecraft. In extreme cases of inhomogeneous charging it can lead to an electrical breakdown between highly charged surfaces. A number of space, laboratory experiments and theoretical studies were made with the aim to investigate the plasma sheath formation and its structure, which depends on a number of parameters, such as geometry, size and potential of body, surface materials, Debye length, Mach number, plasma composition, density and energy of the charged particles, etc. Singh et al. (1987) and Samir et al. (2001) demonstrated that the electrons and ions are heated in the wake, while Siskind et al. (1984) also observed an electron heating in the ram direction. Henderson and Samir (1967) measured the current depletion in the wake with respect to the ram and Samir et al. (1979, 1987) studied the asymmetry in the current distribution in the wake. Oran et al. (1974) observed the increasing of the density in the near-wake region. Although study of the ion collection in the electron-filled wake of a spacecraft was performed during the Charge Hazard and Wake studies' flight experiment onboard shuttles ST-60, ST-69 (Enloe et al., 1997; Davis et al., 1999), the experiment was motivated by a high charging (up to kilovolts) of the low-Earth-orbiting (LEO) spacecraft in the auroral regions which are

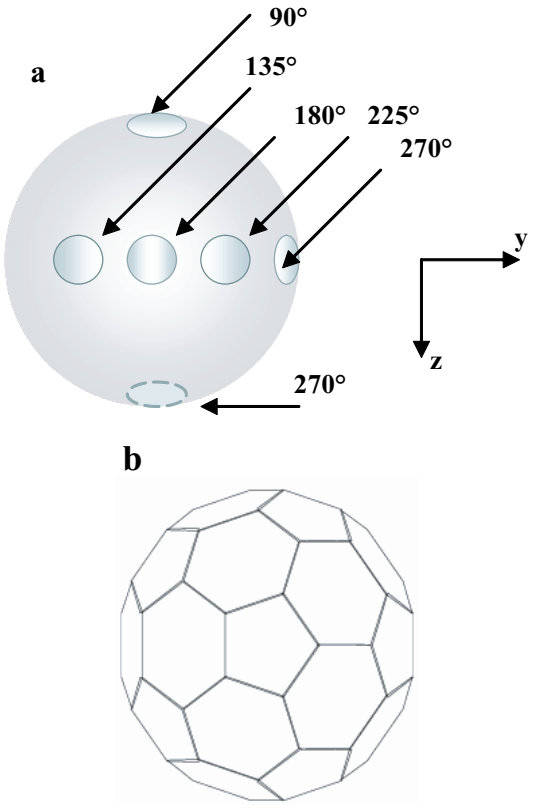

Fig. 1. (**a**) SLP configuration with 6 independent collectors. The symmetry axis of the central collector is aligned with the satellite velocity (along x) and facing the ram. (**b**) Representation of the sphere in the model by an assembly of 12 pentagons and 20 hexagons.

populated with the energetic electrons. They showed that a probe placed in the wake has to be polarized up to 100 V to neutralize the high-energy electron collection. Finally, the influence of the magnetic field on the sheath asymmetries and current collection was investigated by Sanmartin (1970) and Laframboise and Sonmor (1993).

The purpose of this work is to model the current collection by the Segmented Langmuir Probe and to determine its capability to retrieve information on the plasma flow. In its present design (see Fig. 1a), the SLP is a spherical probe 4 cm in diameter with 6 independent spherical caps (∼2 cm in diameter) on its surface. These caps are insulated from each other and from the main probe body and act as individual collectors. They are mounted symmetrically with respect to the orbital velocity direction at angles 90°, 135° and 180° and cover the front part of the probe. Since the SLP is currently flying on the DEMETER CNES micro-satellite at an altitude of about 700 km (see http://demeter.cnrs-orleans.fr), we have limited our analysis to plasma conditions that are encountered in the ionosphere at this altitude by simply taking the ratio of the probe radius r_s to the Debye length λ_D equal to unity. For LEO spacecraft, the thermal ion V_{Ti} and electron V_{Te} velocities and the plasma bulk velocity V_0 in the probe reference frame are such that $V_{Ti} \leq V_0 \ll V_{Te}$. Under these conditions, the plasma flow mainly modifies the angular distribution of the ion current which is controlled by the Mach number and by the potential applied to the probe (Samir et al., 1987). In order to simulate the current collection by the SLP and its collectors, we have developed a PIC (Particles In Cell) electrostatic model which is based on the surface charge distribution method (Renau et al., 1982; Kolesnikova, 1997; Béghin and Kolesnikova, 1998). Our approach differs from the commonly used numerical schemes where the Poisson equation is solved to compute the potential distribution in the sheath. Instead, our algorithm is based on the determination of the volume charges in the sheath and of the surface charges on the probe surface which are subsequently used to obtain the potential distribution in the sheath. This method bears some advantages since the mesh size in the sheath and on the probe can be chosen independently and, more importantly, it allows, at each iteration, a natural control of the total charge neutrality of the probe-sheath system. The computational method is described in more detail in Sect. 2. In Sect. 3, we compare the results for the case of a non-flowing thermal plasma to those published by Laframboise (1966). Section 4 presents the results obtained in the case of a flowing thermal plasma. We briefly evaluate the SLP capabilities to estimate the plasma bulk velocity and present the first onboard measurements in Sect. 5.

2 Description of the model parameters, overview of its main performances

Our model uses the basic principle of PIC codes (see, for example, Procassini et al., 1990) to solve the transport equation. Here, we just briefly explain the main features.

2.1 Size of the simulation box

In order to prevent interferences between the sheath and the boundaries of the simulation box, these boundaries have to be located at a sufficiently large distance from the probe. To obtain an estimate of the extent of the disturbed volume around a spherical obstacle, we consider the simple case of a spherical body at the plasma potential and calculate the density at a distance r from the obstacle of radius r_s by integrating the distribution function and taking into account the geometrical shadow effect of the obstacle on particle trajectories. For example, in a non-flowing isotropic plasma the variation of the density can be written as $n/n_0 = 0.5 \int_{\alpha}^{\pi} \sin\theta d\theta = 0.5 \left(1+\sqrt{1-[r_s/r]^2}\right)$, where n_0 is the undisturbed value, $\alpha = arctg(r_s/r)$ and θ is the spherical angle. The density differs by 2% from the undisturbed value at a distance $\sim 4 r_s$. In the case of a flowing thermal Maxwellian plasma, and neglecting the effects of space charges arising from the differences in ion and electron dynamics, the ion density along the wake axis is given by $n/n_0 = 0.5 \left(1-\Phi(\chi)+\cos\alpha e^{-\chi^2 \sin^2\alpha}(1+\Phi(\chi\cos\alpha))\right)$, where $\chi = V_0/V_T$ is the ion Mach number equal to the

ratio of the bulk velocity V_0 to the thermal ion velocity V_T ($V_T=\sqrt{2kT/m}$, where m is the ion mass, T is the temperature, assumed to be the same for electrons and ions, and Φ is the error function). A similar decrease in the ion density of 2% is reached at a distance of about $9\,r_s$ for $\chi=1$ and $28\,r_s$ for $\chi=4$. The potential applied to the probe significantly modifies the structure and the size of the sheath region. According to Laframboise (1966), in the case of a non-flowing plasma, the disturbed region around a spherical probe of radius $r_s=\lambda_D$ and at a potential $25\,kT/e$ extends to $13\,r_s$.

Taking these numbers into account, the initial size of the simulation box was set to $30\,r_s$ along the flow direction and $15\,r_s$ perpendicular to it. In order to ensure that the size of the simulation box is appropriate, we performed several tests by looking at the variation of the collected currents as a function of the box size. We assume that the box size is adequate, when the current variation for a larger size is less than its fluctuations which arise from the representation of the particle distribution function by a limited number of macro-particles.

2.2 Cell size and time step

In order to ensure computational stability and accuracy of the calculated parameters, the cell size in the simulation box must be about λ_D. The surface of the probe is modelled as an assembly of surface elements under the form of pentagons and hexagons, as shown in Fig. 1b. A correct description of the surface charge distribution and current collection by the cap collectors calls for a size of these pentagons and hexagons similar or smaller than the cap dimension. Given the above constraints, initial runs were performed using a cell size equal to λ_D and, for the pentagons and hexagons, a side length equal to $a\approx 0.4\,r_s$. As will be shown in Sect. 3, we have tested the model accuracy by reducing the cell size to $\lambda_D/2$. Changes in the collected currents appeared to be less than 5%, which is the desired accuracy level of the model determined by the number of macro-particles. In this initial phase of the work and in order to save computation time, we have routinely run the model with a mesh size equal to λ_D.

The travel time τ_e of the electrons through the cells of size λ_D is determined by their thermal velocity V_{Te} and equal to $\tau_e\approx\omega_{pe}^{-1}/\sqrt{2}$, where ω_{pe} is the angular electron plasma frequency. The ions have a thermal velocity $V_{Ti}=\sqrt{m_e/m_i}V_{Te}$ and, in the case of a mesothermal flow, a bulk velocity V_0 of the order of their thermal velocity or a few times more. Their travel time τ_i can be approximated as $\gamma\tau_e$, with $\gamma=\sqrt{m_i/m_e}/(1+V_0/V_{Ti})$, and is thus much larger than the electron one. In order to avoid large density fluctuations within the computation box, the contribution of the macro-particle in each cell, through which it travels, has to be computed. Therefore, the characteristic time has to be small enough to integrate even minor energetic particles, such as particles with the speed (V_0+2V_T), which consist of about 2% of the total population (assuming the electron distribution to be Maxwellian with $T=0.2\,eV$). This leads to a characteristic time of $0.25\omega_{pe}^{-1}$. This requirement is difficult to fulfil due to the large difference between τ_i and τ_e. Since we are looking for a stationary solution, we adopted the technique of the numerical time step (Jolivet and Roussel, 2002; Roussel and Berthelier, 2004) with two different integration time steps for ions τ_i and electrons τ_e, respectively.

The current collected by a surface element during the corresponding time step τ_k is calculated as $j=-\sum_i q_k N_k/\tau_k$, where q_k is the species charge (negative for electrons and positive for ions), N_k is the number of particles of the k-species. The computation is stopped when the computed parameters (potential, charge densities, currents) reach a stationary state and the total charge in the probe-sheath system is zero.

2.3 Particles injection

Potential at the boundaries of the simulation box is set to 0 and particles are injected at each time step under the form of randomly generated macro-particles, in order to reproduce an undisturbed distribution function. From the experience gained during initial tests of the model the number of macro-particles was chosen such as to provide 180 particles of each species in each cell close to the boundaries, which ensures sufficiently low fluctuations of the computed parameters (i.e. less than 5% of their equilibrium values). To reduce numerically generated disturbances in the ion and electron plasma density close to the boundaries (see, for example, Roussel and Berthelier, 2004), the macro-particles are actually injected from a pre-box region of extent $\lambda_D/2$ with a uniform spatial distribution.

2.4 Computation of the volume and surface charges

To compute the charges deposited in the volume cells of the simulation box by the macro-particles, each of them is considered as a cube of dimension λ_D with a uniform charge density. The macro-particle contribution to each of the 8 adjacent cells is taken in proportion to the common volume of this cube with the cell itself. The potential at the centre of any element k, be it a volume or a surface element, is expressed as a sum of the individual contributions due (i) to the charges on the surface elements $i\neq k$, (ii) to the volume charges in the cells $j\neq k$ and (iii) to the charges of the element k itself, i.e.

$$\varphi_k=\sum_{i\neq k}\frac{q_{si}}{4\pi\varepsilon_0 r_{ik}}+\sum_{j\neq k}\frac{q_{vj}}{4\pi\varepsilon_0 r_{jk}}+\frac{q_k}{4\pi\varepsilon_0}\phi_{kk}. \quad (1)$$

Here the charge q of any element is supposed to be located at the centre of mass of the element, r_{lm} is the distance between the centres of the elements l and m, and s_k (v_k) is the surface (volume) of the element. The last term represents the contribution of the charge of the element k itself, which may be written (see Kolesnikova, 1997) as $\phi_{kk}=\frac{1}{s_k}\iint_{s_k}\frac{ds}{\rho_k}$ for a surface element and $\phi_{kk}=\frac{1}{v_k}\iiint_{v_k}\frac{dv}{\rho_k}$ for a volume element. The charge distribution inside the element is considered to be uniform; ρ_k is the distance between the centre of mass

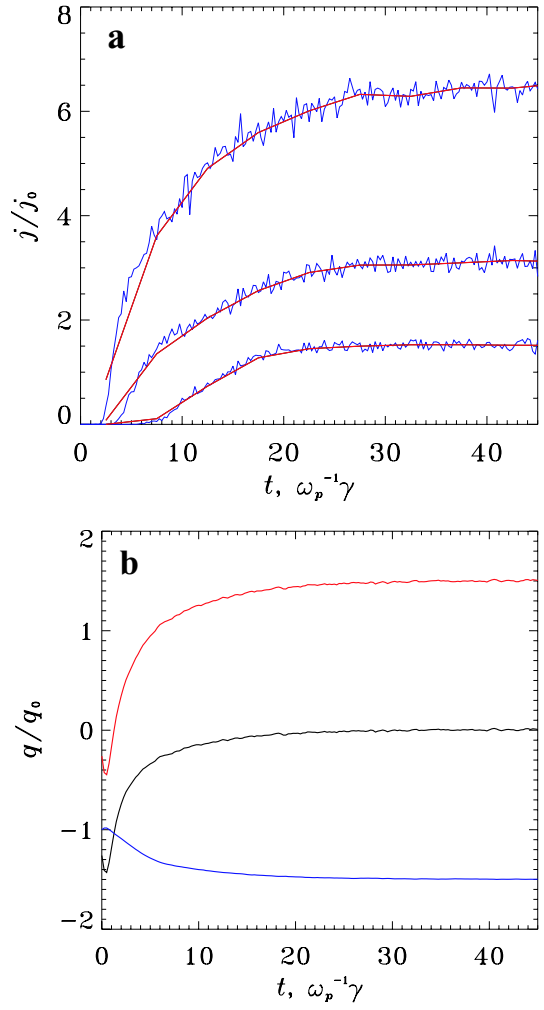

Fig. 2. (**a**) Ion current collected by spherical probe in the case $\varphi=-20\,kT/e$, $\lambda_D=r_s=2$ cm, $T_e=T_i=T=0.2\,eV$. The current is normalised by its value $j_0=2\sqrt{\pi}er_s^2nV_T$ at $\varphi=0\,V$. Upper, middle and lower curves correspond, respectively, to an H^+ plasma with $V_0=V_{Ti}$, $V_0=2V_{Ti}$ and to an O^+ plasma with $V_0=4V_{Ti}$. Blue lines represent calculated values of the ion current at each iteration and red lines represent their averages over a period of $5\gamma\omega_{pe}^{-1}$. (**b**) Variation of the total volume (red line) and surface (blue line) charges for the case $V_0=V_{Ti}$. Global charge of the system is shown in black. Charges are normalised by the surface charge in a vacuum.

and a given position. Once the volume charges in the cells are determined, surface charges are computed from the linear system obtained by using expression Eq. (1) for each surface element k and the condition that the potential on the surface is equal to the desired value Φ. The complete set of volume and surface charges is then used to compute the electric field inside the simulation box which controls the particles motion during the next iteration.

In our model, the sphere is represented (Fig. 1b) by a set of 12 pentagons and 20 hexagons with a side $a\approx0.4\,r_s$, for which $\phi_{kk}=\frac{4}{a}\ln[(\sin\beta+1)/\cos\beta]$, with $\beta=36°$ and $30°$, respectively. For the simple case of a sphere in vacuum, this entails an underestimate of the total charge by about 5% compared to the true value $4\pi\varepsilon_0 r_s$. The same ratio between actual and computed charges must also hold in the presence of a sheath since this is only a geometrical effect. This factor is taken into account by multiplying the contributions of the surface charges by 1.05 in Eq. (1).

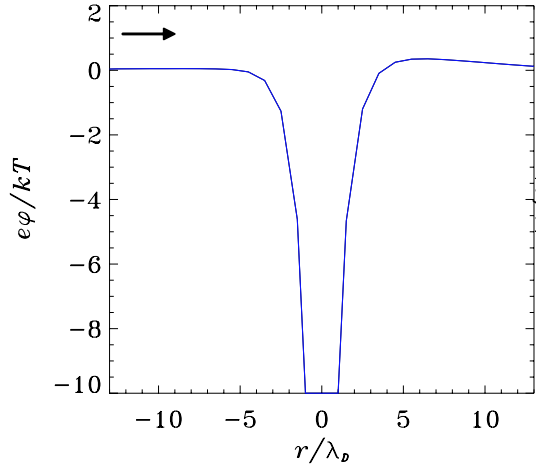

Fig. 3. Potential distribution along the x-axis parallel to the bulk velocity in an O^+ plasma with $V_0=4V_{Ti}$. Plasma parameters and probe potential are the same as in Fig. 2, where the potential is normalised by plasma temperature. Direction of the bulk velocity is indicated by an arrow.

2.5 Performances overview

In order to illustrate the above discussion, we present in Fig. 2 the evolution of the total ion current collected by the probe and of the total space and surface charges as a function of the simulation elapsed time. These results were obtained for a probe polarised at a negative potential $\varphi=-20\,kT/e$ in a plasma with $\lambda_D=r_s=2$ cm and $T_i=T_e=T=0.2\,eV$. The current is normalized with respect to its value at $0V$, i.e. $j_0=2\sqrt{\pi}er_s^2\,nV_T$. Upper, middle and lower curves in Fig. 2a correspond to a H^+ plasma with a bulk velocity $V_0=V_{Ti}$, $V_0=2V_{Ti}$ and to an O^+ plasma with $V_0=4V_{Ti}$, respectively. Computed values of the ion current are shown in blue, whereas their average over a period equal to $5\gamma\omega_{pe}^{-1}$ is shown in red. In all cases, currents reach a stationary state at $\sim30\gamma\omega_{pe}^{-1}$, well before the end of the simulation ($45\gamma\omega_{pe}^{-1}$). Figure 2b displays the evolution of the total charge in the sheath (in red), the total charge on the probe surface (in blue) and the global charge in the system (in black) in H^+ plasma with $V_0=V_{Ti}$. The charges are normalized with respect to the surface charge of the spherical probe in a vacuum, i.e. $4\pi\varepsilon_0 r_s\varphi$. The global charge neutrality of the probe-sheath system is reached at $\sim30\gamma\omega_{pe}^{-1}$ and persists thereafter with an accuracy better than 1%.

An example of the potential distribution along the x-axis parallel to the bulk velocity is shown in Fig. 3 for an O^+ plasma with $V_0=4V_{Ti}$. Plasma parameters and probe potential are the same as in the above Fig. 2. The potential is nearly constant and equal to 0 (potential in the undisturbed plasma)

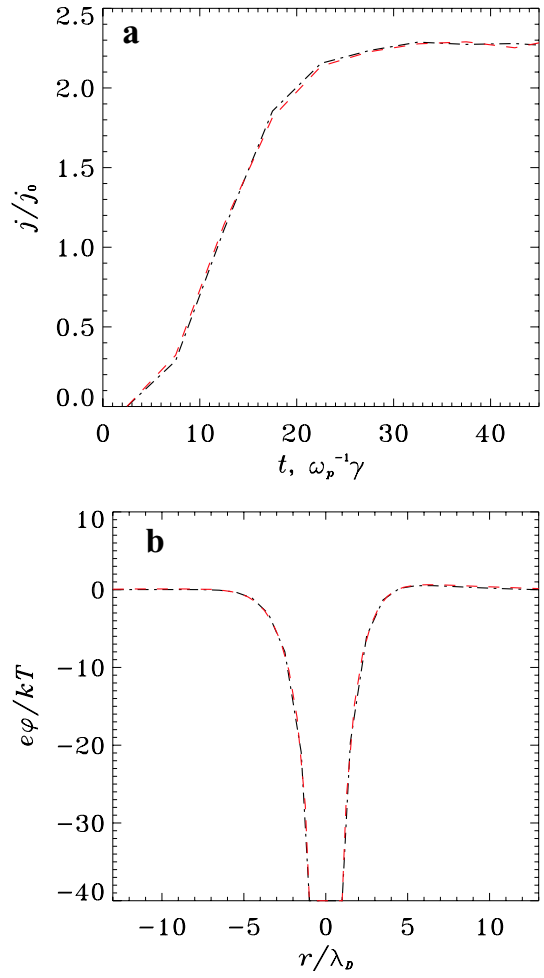

Fig. 4. **(a)** Ion current averaged over a period of $5\gamma\omega_{pe}^{-1}$; **(b)** potential distribution along the x-axis parallel to the bulk velocity in the case of O^+ plasma with $V_0{=}4V_{Ti}$, $\lambda_D{=}r_s{=}2$ cm, $T{=}0.1\,eV$, $\varphi{=}{-}40\,kT/e$. Red and black lines stand for the results of the model with the cell size of $\lambda_D/2$ and λ_D, respectively.

at distances from the probe surface larger than $\sim 7\,r_s$ on the front side and $\sim 9\,r_s$ in the wake. Its continuity with the potential in the undisturbed plasma demonstrates that the size of the simulation box is adequate.

Finally, we have presented in Fig. 4 results obtained for two different dimensions of the cell sizes in the simulation box, namely λ_D (in back) and $\lambda_D/2$ (in red), in the conditions $\varphi{=}{-}40\,kT/e$, $\lambda_D{=}r_s{=}2$ cm and $T{=}0.1\,eV$ for O^+ plasma with $V_0{=}4V_{Ti}$. Differences in the total current (Fig. 4a) and in the potential distribution in the sheath (Fig. 4b) are negligible. The angular current distribution for the $\lambda_D/2$ mesh size is compared to that for the λ_D mesh size in Fig. 12 of Sect. 4. Again no significant difference is noticeable. For this reason, we use in the following a λ_D mesh size which allows much faster computation without any significant loss of accuracy.

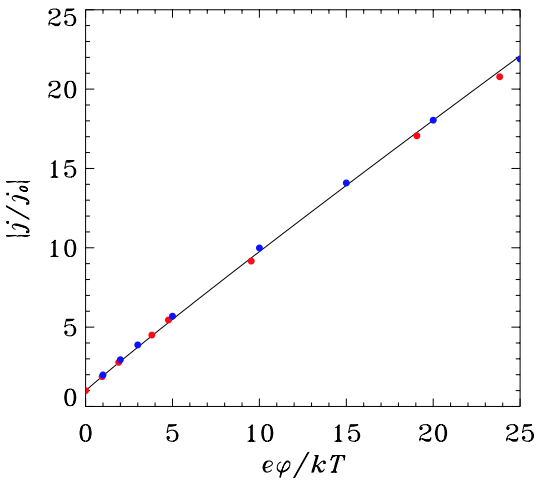

Fig. 5. Normalised current as a function of normalised attractive potential of a spherical probe of radius r_s=2 cm in a non-flowing plasma with λ_D=2 cm and $T_e{=}T_i{=}0.2\,eV$. Results of Laframboise (1966) are shown as blue dots, model results are shown as red dots.

3 Probe response in a non-flowing isotropic plasma and model validation

In order to validate our model, we compare the results with those given by Laframboise (1966), who developed an iterative method for the numerical steady-state solution of the Poisson equation and the collisionless Boltzmann equation in thermal non-flowing plasma in spherical and cylindrical symmetries. We consider the case of a spherical probe in a plasma with the following characteristics: electron density $2.8{\cdot}10^4$ cm^{-3}, equal ion and electron temperatures $T_e{=}T_i{=}T{=}0.2\,eV$, corresponding to a Debye length $\lambda_D{=}2$ cm, and a ratio r_s/λ_D equal to 1. Figure 5 shows a comparison between the total current collected by the sphere as obtained with our model (red dots) and with that of Laframboise (blue dots), for several values of the probe potential. The potential is normalized to the temperature and the current to its value at plasma potential. Clearly, currents given by the two models are in excellent agreement. In Fig. 6 we have compared the structure of the sheath obtained in the two models by plotting (a) the electron (in red) and ion (in blue) charge densities in the sheath and (b) the potential. The Laframboise solution is shown as a solid line and results from our model are represented by dots. Again, the good agreement between the two sets of results validates our numerical model, in particular the choice of its parameters (size of the simulation box, space and surface elements, integration time etc.).

4 Probe response in a flowing plasma

The plasma bulk velocity produces an asymmetry of the charge distribution in the sheath region and the formation of a wake behind the probe. It therefore modifies the current

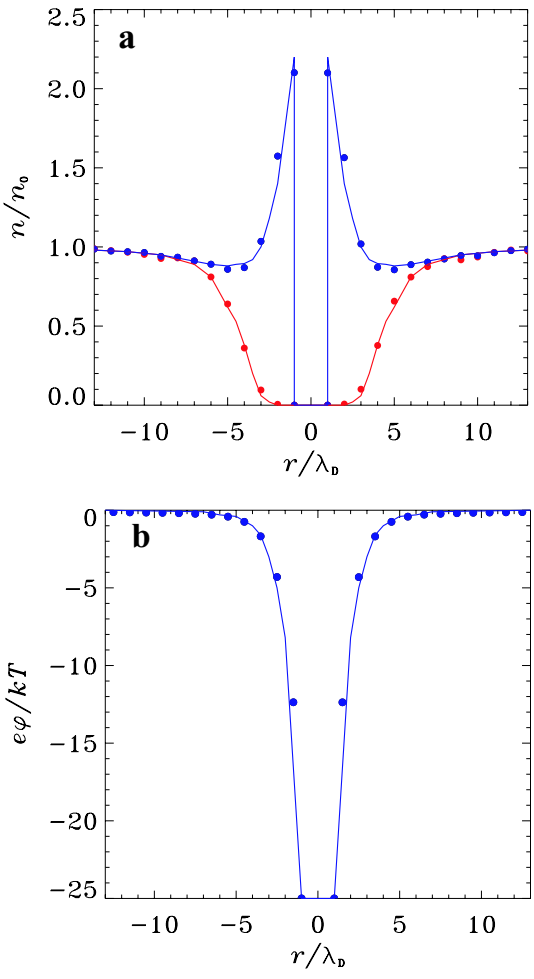

Fig. 6. **(a)** Density distribution around the spherical probe for attracted (blue) and repelled (red) particles; **(b)** potential profile in the sheath in the case of a non-flowing plasma with λ_D=r_s=2 cm, probe potential φ=$-25\,kT/e$. Results of Laframboise are shown by solid lines and the model solution by dots. Charge densities are normalised by their values in the undisturbed plasma, distances by the Debye length, potentials by plasma temperature.

collection, leading to an asymmetry of the current distribution over the probe surface. In the case of satellite observations in the ionosphere, the bulk velocity mainly arises from the satellite orbital speed (7.5 km s^{-1} for a circular orbit at an altitude of 700 km), while the drift velocity in the Earth's reference frame amounts to only about $\leq$15% of the plasma velocity in the probe reference frame. Under the considered plasma conditions, the drift velocity is much smaller than the electron thermal velocity (267 km s^{-1}). It is of the same order of magnitude as the H^+ thermal velocity (6.2 km s^{-1}) and a few times larger than the O^+ thermal velocity (1.5 km s^{-1}). Therefore, the plasma flow will mainly modify the ion branch of the collected current. This is why we focus on the case of a negatively polarised probe.

Shown in Fig. 7 are the variations of the current on the entire sphere as a function of the probe potential for an H^+ plasma with the same parameters as above and with 3 differ-

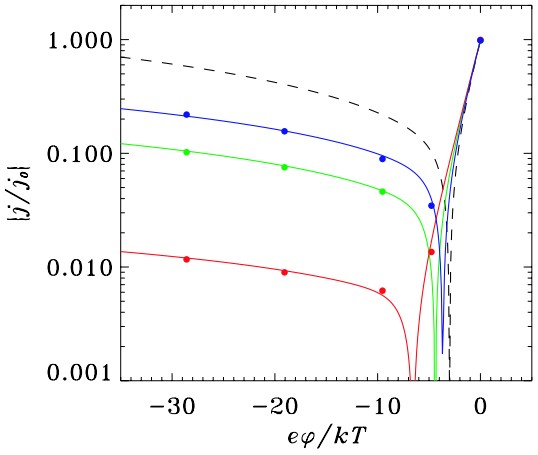

Fig. 7. Normalised current versus normalised potential in an H^+ plasma with V_0=0 (black), V_0=V_{Ti} (blue), V_0=2V_{Ti} (green) and in the O^+ plasma with V_0= 4V_{Ti} . Dots stand for the computed values and their fit is shown as a solid line. Plasma and probe characteristics are identical as in Fig. 2.

ent Mach numbers χ=V_0/V_T (i.e. 0 (non flowing plasma, in black), 1 (blue), 2 (green)) and for an O^+ plasma with χ=4 (red). Dots are used to indicate the computed values and an empirical best fit by a function of the form $\alpha(1-e\varphi/kT)^\beta$ is shown as a solid line. The ion branch of the collected current extends from the lowest value of the applied potential ($-35\,kT_e$) to the floating potential φ_f, which is a few kT_e negative (for example, $-6\,kT_e$ for the O+ plasma). In this range, the attracting probe potential is much larger than the H^+ energy (0.2 eV for χ=1 and 0.8 eV for χ=2) and an order of magnitude larger than the kinetic energy of the oxygen (3.2 eV). The electron branch of the ion-voltage characteristics extends above the floating potential. The ion currents vary approximately as $\chi^{-1}[m_i/m_p]^{-0.5}$ and, therefore, the total ion current decreases due to (i) an increase in the bulk velocity with respect to the thermal velocity or (ii) an increase in the heavy ion concentration.

The angular distribution of the current collected over the probe surface is controlled by the direction of the plasma flow which determines the symmetry axis of the current distribution. In addition, the current distribution also depends on the ratio between the ion bulk energy and the attracting potential of the polarized probe and also on the ion Mach number. Ions with a large bulk velocity and which travel along trajectories that do not intersect the probe do not get in the wake if their bulk energy is much larger than the attracting potential. However, a high thermal velocity (hence a low Mach number) modifies this situation by diffusing the ions into the wake. Under the action of the electric field in the sheath, the ions will be accelerated in the front part of the sheath (which faces the flow direction) and will be slowed down in the rear part of the sheath. Therefore, the front part of the sheath will have a lack of positive charge, due to the ion large velocity, compared to the rear part where the ions are slowed and their density is increased accordingly.

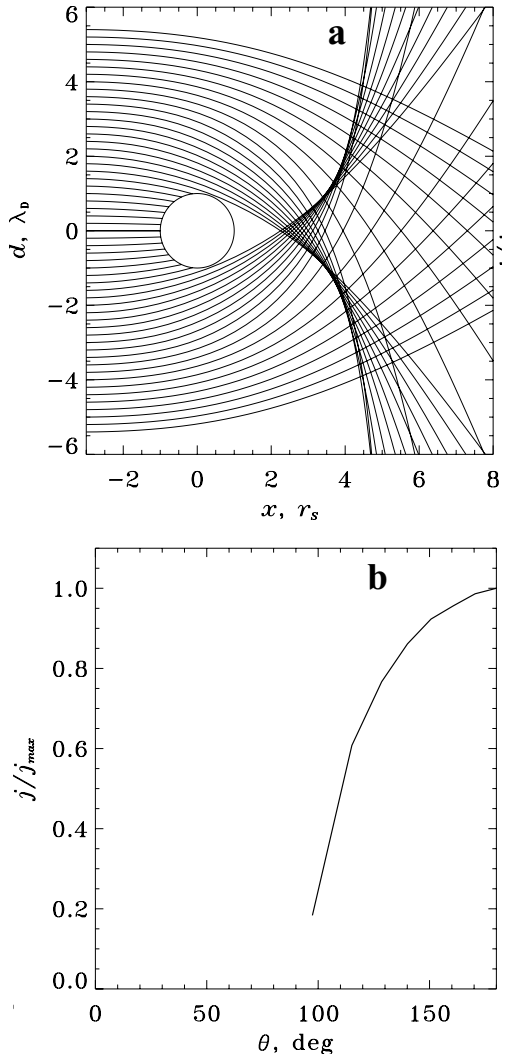

Fig. 8. (a) Trajectories of O^+ ions in a cold beam model with velocity equal to $6.2 \cdot 10^3\,\mathrm{m\,s^{-1}}$ in the field of the negatively polarised sphere with φ=−4 V; **(b)** corresponding current angular distribution, θ is the angle between the velocity vector and the outward normal to the probe surface.

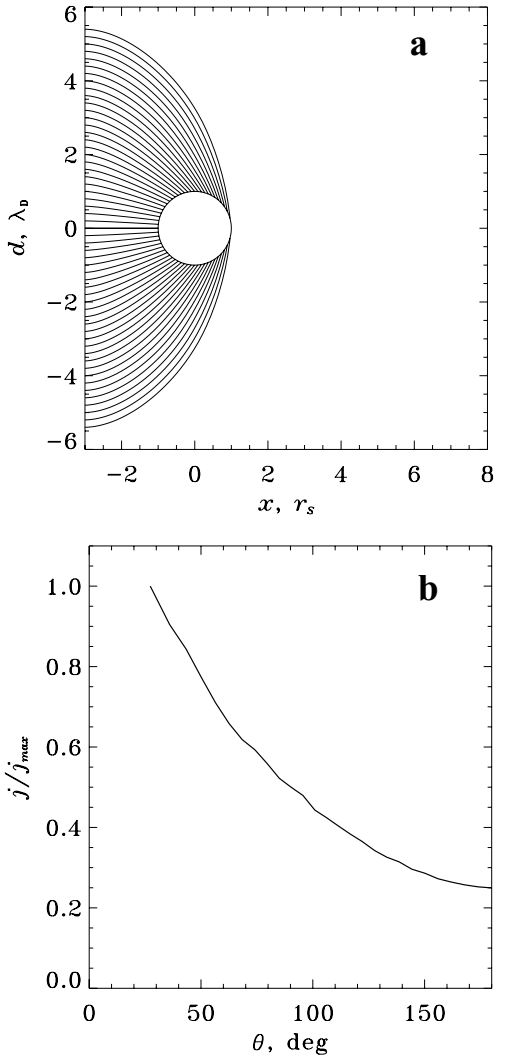

Fig. 9. (a) Trajectories of H^+ ions and **(b)** corresponding current angular distribution over the probe surface. Conditions are identical to those in Fig. 8.

In order to illustrate the physics of the problem, we consider the case of a cold ion beam that flows towards a negatively polarized probe. To mimic the role of the attracting electric field in the sheath, we take a constant electric field equal to $0.45\varphi/r_s$ around the probe, up to a distance of 2 r_s and decreasing as r_s^{-2} at larger radial distances. Although fairly simple, this model adequately describes the influence of the field on ion trajectories around a negatively polarized sphere with r_s=λ_D. Trajectories of O^+ ions with a bulk velocity of $6.2 \cdot 10^3\,\mathrm{m\,s^{-1}}$ that move in such a field are shown in Fig. 8a in the case of a sphere potential φ=−4V. The ions move from left to right and their trajectories are launched with a uniform distribution at the plane x=−3r_s. The attracting electric field of the probe focuses the ions in a range of 2.3 to 3.5 r_s in the wake. Particles that cross the plane x=−3r_s at a distance from the x-axis, between d_1 and d_2, carry a current which is proportional to $\pi\,|d_2^2-d_1^2|$. If these particles hit the sphere surface over an angular sector defined by the angles θ_1 and θ_2 (where θ is the angle between the particle velocity and the outward normal to the probe surface), the current density in this sector will be proportional to $0.5\,|d_2^2-d_1^2|\,r_s^{-2}\,|\cos\theta_1-\cos\theta_2|^{-1}$. The angular distribution of the current over the entire surface can be obtained by applying this formula to pairs of neighbouring trajectories. As an example, Fig. 8b displays the current distribution versus angle θ obtained from trajectories shown in Fig. 8a. The current reaches its maximum on the front part of the spherical probe (θ=180°) and drops down quasi exponentially when θ decreases. For light ions, such as H^+, the situation is different, as is illustrated in Fig. 9, which displays (a) the ion trajectories and (b) the resulting current distribution. The attracting potential of the probe (20 times greater than the ion bulk energy) attracts all particles with initial trajectories

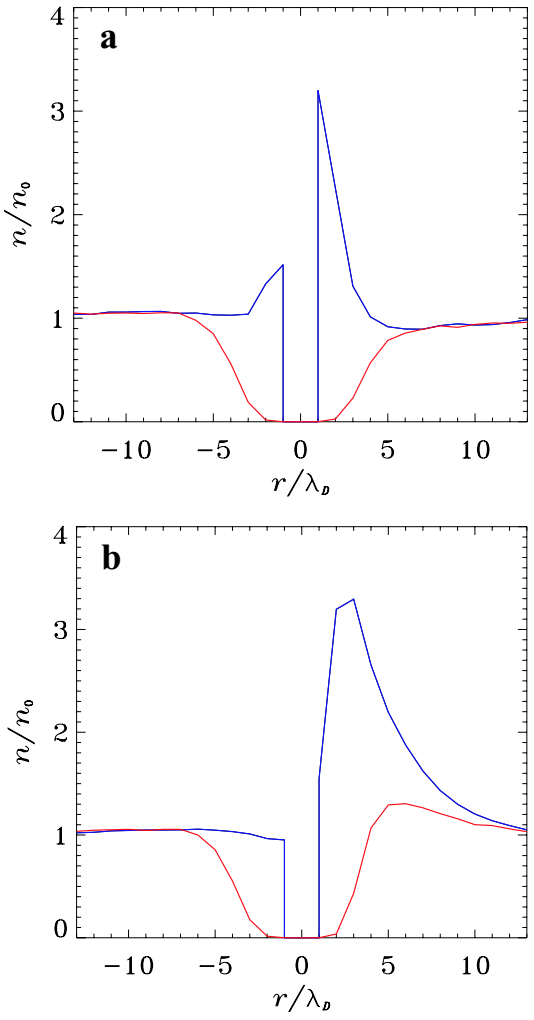

Fig. 10. Positive (blue) and negative (red) charge densities along the $x-$axis parallel to the flow velocity for $\varphi=-20\,kT/e$ **(a)** in an H^+ plasma with $V_0=V_{Ti}$ and **(b)** in an O^+ plasma with $V_0=4V_{Ti}$. Plasma and probe parameters are the same as in Fig. 2. Charges are normalised by their values in the undisturbed plasma, distances by the Debye length.

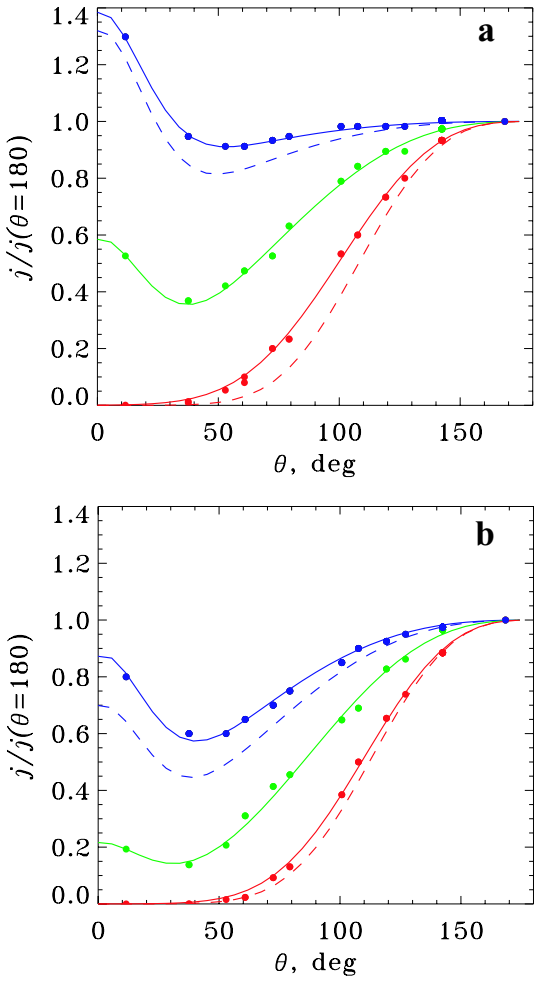

Fig. 11. Current angular distribution in an H^+ plasma with $V_0=V_{Ti}$ (blue), V_0=1.3 V_{Ti} (blue dashed), V_0=2 V_{Ti} (green) and in an O^+ plasma with $V_0=4V_{Ti}$ (red),V_0=5.2 V_{Ti} (red dashed). Dots indicate computed values, solid lines represent their fits. Currents are normalized to their values for θ=180°. Plasma and probe characteristics are the same as in Fig. 2 and **(a)** $\varphi=-20\,kT/e$, **(b)** $\varphi=-10\,kT/e$.

within 5.5 r_s from the $x-$axis. As seen in Fig. 9a, the density of trajectories that hit the probe surface increases when the impact location on the sphere moves from the front to the wake side. As a result, the current follows the same behaviour (Fig. 9b).

In a plasma with a non-zero temperature, the thermal velocity will modify the current collection by the probe, especially in the case of light ions with a smaller Mach number than that of heavy ions. Nevertheless, we may expect that the main feature of the cold plasma model, i.e. a strong decrease of the current on the rear part of the probe for heavy ions and an increase of the current on this rear part for light ions, is still conserved. The results obtained from our model are presented in Fig. 10, which shows the charge density distribution of electrons (red line) and ions (blue line) along the $x-$axis for the conditions T=0.2 eV, $r_s=\lambda_D$=2 cm, $\varphi=-20\,kT/e$ (a) in a H^+ plasma with $V_0=V_{Ti}$ and (b) in an O^+ plasma with $V_0=4V_{Ti}$. The maximum of the ion density in the wake region is found to be located just in the vicinity of the probe surface for the H^+ plasma and between 2–3λ_D in the O^+ plasma. These results are in agreement with the simple cold beam model. As mentioned in the beginning of this paragraph, the ion space charge density is greater in the wake than on the front sheath, owing to the effect of the ion slowing in the near wake and to their accelerating in the front.

The computed angular distributions of the current are shown in Fig. 11 for five cases, i.e. $V_0=V_{Ti}$ (blue), V_0=1.3 V_{Ti} (blue dashed), V_0=2 V_{Ti} (green) in the H^+ plasma and V_0=4 V_{Ti} (red), V_0=5.2 V_{Ti} (red dashed) in the O^+ plasma. Plasma conditions are identical to those in Fig. 10 and the probe potential is set to $\varphi=-20\,kT/e$ and $\varphi=-10\,kT/e$, respectively, in Figs. 11a and b. Dots show the

computed values and their fit by an exponential law is shown as a solid line. Currents are normalized to their values for θ=180°. The current distribution in the O^+ plasma is nearly the same as that obtained from the simple cold beam model, with a maximum at 180° and an exponential decrease when θ decreases. The current collected by the probe on its sector facing the wake does not show any effect due to the increase of the ion space charge density along the wake direction close to the probe surface. This is due to the fact that the negative probe potential is not large enough to attract them. In the front side, the current distribution in the H^+ plasma with V_0=V_{Ti} differs from that predicted by the cold beam model. The current is maximum for the ram direction (θ=180°) and does not show any significant decrease over a large sector of the front face (up to θ=100°), the distribution being thus very close to that of a non-flowing isotropic plasma. In the rear side (θ<90°), the current, which decreases up to θ angles of about 45°, increases then and displays a maximum along the wake direction. In this case the potential of the probe is large enough to attract the ions accumulated in the wake. If the H^+ bulk velocity is increased or if the attracting potential is decreased (both effects resulting in a decrease in the ratio between the attracting potential and the ion bulk energy), the current distribution then becomes narrower on the front side and the current is reduced on the rear side. At this stage, it is interesting to note that accurate measurements of the current angular distribution in the rear side of the probe for several probe potentials could provide a way to disentangle the two competing parameters that control the current distribution, i.e. the bulk velocity and the ion composition, and possibly to retrieve these two parameters.

As mentioned in Sect. 2, we present in Fig. 12 a comparison of the angular distribution of the current obtained in the case of an O^+ plasma for two mesh sizes in the simulation box, λ_D and $\lambda_D/2$. The differences between these two curves are minor and within the accuracy of the model which validates the use of a λ_D mesh size.

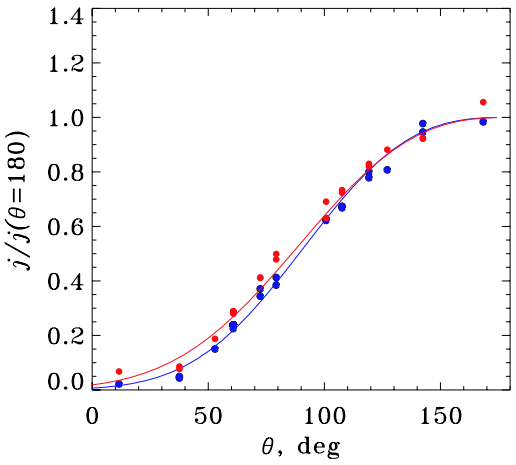

Fig. 12. Current angular distribution in an O^+ plasma with V_0=4V_{Ti}, λ_D=r_s=2 cm, T=0.1 eV, φ=−40 kT/e. Red and blue lines stand for the results of the model with the cell size of $\lambda_D/2$ and λ_D, respectively. Currents are normalized to their values for θ=180°.

5 Preliminary evaluation of the probe capability to deduce the plasma bulk velocity

Instruments that are well suited to measure ion velocities in the ionosphere are based on a combination of a drift meter and a retarding potential analyser. This technique was proposed many years ago through the pioneering work of W.B. Hanson (see, for example, Hanson et al., 1973; Hanson and Heelis, 1975; Heelis et al., 1981). Careful data reduction algorithms (Hanson and Heelis, 1998; Séran, 2003) can provide the ion flow velocity with an accuracy as good as $\sim\pm10\,m\,s^{-1}$ for the transverse velocity and ±10% for the ram velocity. The goal of the Segmented Langmuir Probe (SLP) is to use the Langmuir probe as an alternative tool to deduce the ion bulk velocity, in addition to the routinely measured electron density and temperature. It is clear that an accuracy as good as that provided by the ion analyzer technique is probably out of reach, at least at the present stage of development of the instrument. Nevertheless, the SLP has two interesting advantages, i.e. (i) it also provides the thermal electron parameters, (ii) it only requires modest spacecraft resources in terms of mass, volume, power and, more importantly, attitude control. This can be of interest for planetary missions, for example, where a modest accuracy in the determination of plasma velocity would be sufficient.

Let us briefly examine the SLP capabilities to derive the ion flow velocity based on the initial results of our model. Consider the case of an O^+ plasma, since this is the major ion during daytime at terrestrial mid latitudes, as well as in the auroral and polar regions at ∼700 km altitude, and look separately at the effects of a component of the ionospheric plasma velocity (i) perpendicular or (ii) parallel to the satellite orbital velocity. In the SLP configuration onboard DEMETER, the surface collectors are located on the front and side parts of the probe, i.e. at angles of 180°, 135° and 90° (Fig. 1a) with respect to the orbital velocity. Figure 11 demonstrates that the angular variation of the normalized current in the [90°, 135°] angular range is about 0.01/deg in the O^+ plasma and two times less in the H^+ plasma. Taking into account the predicted accuracy of about $5{\cdot}10^{-3}$ of the current measurements by the SLP collectors, a change by 1° of the flow velocity direction perpendicular to the symmetry axis of the probe appears to be a reasonable sensitivity limit. Such a change in the flow direction corresponds to a velocity component of the ionospheric plasma of $130\,m\,s^{-1}$ perpendicular to the satellite velocity along a 700-km circular orbit. A variation of the ionospheric plasma bulk velocity component parallel to the satellite orbital velocity of $1860\,m\,s^{-1}$ (Fig. 11a) induces a change in the ratio between the 180° and 90° collector of 14%. From the measurement accuracy ($5{\cdot}10^{-3}$), we can therefore estimate that the SLP should be able to detect an ionospheric plasma velocity of $66\,m\,s^{-1}$ along the axis of the satellite orbital velocity. To obtain these simple estimates,

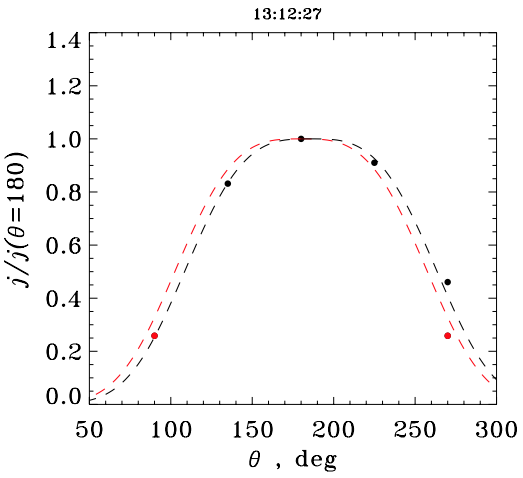

Fig. 13. Currents measured by SLP in the night sector at $-50°$ magnetic latitude in the conditions $\lambda_D \approx 2$ cm, $T \approx 0.15\,eV$, $e\varphi = -20\,kT$. Black and red dots stand for the currents measured in the plan xoy and xoz, respectively. Currents are normalized to the current recorded by the segment located at 180°. The red dashed line is the same as that which is presented in the Fig. 11a, the black dashed line is the same as the red one but is shifted along θ-axis by 6°.

we assumed that the only species in the ionospheric plasma is O^+ and that the ion temperature is known. Although the SLP onboard Demeter is not routinely operated, there are a few orbits when it made the measurements. We present the currents measured by individual segments of the SLP in plasma conditions which are close to those considered in our paper, i.e. $\lambda_D \approx 2$ cm, $T \approx 0.15\,eV$. These observations were made on 2 October 2004 in the night-side sector at about $-50°$ magnetic latitude. Black and red dots in Fig. 13 stand for the currents measured in the plan xoy and xoz, respectively. All currents are measured in the case $e\varphi = -20kT$ (like in Fig. 11a) and are normalized to the current collected by the segment located at 180°, the normal of which is parallel to the satellite velocity. The red dashed line is the same as that which is presented in the Fig. 11a and is used to fit the current distribution in the case of O^+ plasma flowing with the velocity $V_0 = 4V_T(O^+)$ with respect to the probe. The black dashed line is the same as the red one but is shifted by 6° along the θ-axis. These measurements show a really good agreement with our model.

Of course, more work needs to be done to study in details the operation of the SLP and to evaluate its performance in the domain of ion velocity measurements. It should be interesting, in particular, to study if the SLP can directly provide measurements of the ion temperature and of the ion composition, as mentioned in Sect. 4. There are also a number of effects that have not been considered, such as the influence of the magnetic field or the photoelectron emission due to solar UV, which may create additional asymmetries and modify the current collection.

6 Conclusion

We have built a PIC numerical model that is well adapted to the problem of current collection by the Segmented Langmuir Probe, which is part of the scientific payload the DEMETER micro-satellite. With the aim to validate our numerical model and its accuracy, we compared our results with those obtained by Laframboise (1966) in a non-flowing thermal plasma and found a very good agreement. Extension of the model in the case of a flowing plasma under conditions $V_T(O^+) < V_T(H^+) \approx V_0 \ll V_{Te}$ has allowed us to demonstrate that the current collection of a negatively polarized probe is very different for heavy (O^+) and light (H^+) ions:

- even a minor H^+ density results in a significant increase of the total current;
- the current distribution on the front part of the spherical probe steeply decreases with the angle in an O^+ plasma and is practically uniform in an H^+ plasma;
- the H^+ ions are attracted in the wake and contribute significantly to the current collection on the wake side of the probe.

Taking into account the predicted accuracy of the current measurements by the SLP collectors, we conclude that a plasma velocity of about $150\,m\,s^{-1}$ perpendicular to the satellite orbital velocity can be resolved from the SLP measurements in an O^+ plasma, while this threshold increases to $\sim 250\,m\,s^{-1}$ in a H^+ plasma.

First observations made by the SLP onboard Demeter in plasma conditions similar to those considered in this paper show a good agreement with our model. More work remains to be done to investigate in detail the operation of the SLP in different plasma conditions.

Acknowledgements. This work was supported by contracts 04/CNES/1589/DEMETER and ESA/ESTEC/42-2003.

Topical Editor M. Lester thanks a referee for his/her help in evalauting this paper.

References

Al'pert, Y. L.: Waves and artificial bodies in near-Earth plasma, in Russian, Nauka, Moscow, 1974.

Béghin, C. and Kolesnikova, E.: The Surface-Charge Distribution approach for modellization of quasistatic electric antennas in isotropic thermal plasma, Radio Sci., 33, 503–516, 1998.

Davis, V. A., Mandell, M. J., Cooke, D. L., and Enloe, C. L.: High-voltage interactions in plasma wakes: Simulation and flight measurements from the Charge Hazards and Wake Studies (CHAWS) experiment, , J. Geophys. Res., 104, 12 445–12 459, 1999.

Enloe, C. L., Cooke, D. L., and Pakula, W. A. et al.: High-voltage interactions in plasma wakes: Results from the charging hazards and wake studies (CHAWS) flight experiments, J. Geophys. Res., 102, 425–433, 1997.

Hanson, W. B., Zucarro, D. R., Lippincott C. R., and Sanatani, S.: The retarding potential analyzer on Atmosphere Explorer C, Radio Sci., 8, 333–339, 1973.

Hanson W. B. and Heelis, R. A.: Techniques for measuring bulk gas-motions from satellites, Space Sci. Instrum., 1, 493–524, 1975.

Hastings, D. and Garrett, H.: Spacecraft environment interactions, Cambridge atmospheric and space science series, 1996.

Heelis, R. A., Hanson, W. B., Lippincott, C. R., Zucarro, D. R., Harmon, L. L., Holt, B. J., Doherty, J. E., and Power, R. A.: The ion drift meter for Dynamics Explorer-B, Space Sci. Instrum., 5, 511–520, 1981.

Heelis, R. A. and Hanson, W. B: Measurements of thermal ion drift velocity and temperature using planar sensors, in: Measurement techniques in space plasmas, particles, edited by: Pfaff, R. F., Borovsky, J. E., and Young, D. T., American Geophysical Union, Washington, 61–71, 1998.

Henderson, C. I. and Samir, U.: Observations of the disturbed region around an ionospheric spacecraft , Planet. Space Sci., 15, 1499–1513, 1967.

Jolivet L. and Roussel, J. F.: Numerical simulation of plasma sheath phenomenon in the presence of secondary electronic emission, IEEE Trans. Plasma Sci., 30, 318–325, 2002.

Kolesnikova, E.: Méthode des distributions superficielles de charges pour la modélisation des antennes électriques en plasma homogène, isotrope et Maxwellien, Thèse de Doctorat, Univ. Orléans, 1997.

Laframboise, J. G.: Theory of spherical and cylindrical Langmuir probes in a collisionless, Maxwellian plasma at rest, UTIAS report N 100, Institute for aerospace studies, University of Toronto, 1966.

Laframboise, J. G. and Sonmor, L. J.: Current collection by probes and electrodes in space magnetoplasma : a review, J. Geophys. Res., 98, 337–357, 1993.

Lebreton, J.-P.: Micro-satellite DEMETER, DCI-ISL, Technical note, ESTEC SCI-SO, 2002.

Oran, W. A., Stone, N. H., and Samir, U.: Parametric study of near-wake structure of spherical and cylindrical bodies in the laboratory, Planet. Space Sci., 379–390, 1974.

Procassini, R. J., Birdsall, C. K., and Morse, E. C.: A fully kinetic, self-consistent particle simulation model of the collisionless plasma-sheath region, Phys. Fluids B, 2, 3191–3204, 1990.

Renau, A., Read, F. H., and Brunt, J. N. H.: The charge-density method of solving electrostatic problems with and without the inclusion of space-charge, J. Phys. E: Sci. Instrum., 15, 347–356, 1982.

Roussel, J. F. and Berthelier, J.-J.: A study of the electrical charging of the Rosetta orbiter: 1. Numerical model, J. Geophys. Res., 109(A01104) doi:10.1029/2003JA009836, 2004.

Sanmartin, J. R.: Theory of a probe in a strong magnetic field, Phys. Fluids, 13, 103–116, 1970.

Samir, U., Gordon, R., Brace, L., and Theis, R.: The near wake structure of the Atmospheric Explorer C (AE-C) satellite: A parametric investigation, J. Geophys. Res., 84, 513–522, 1979.

Samir, U., Comfort, R. H., Wright, K. H., and Stone, N. H.: Intercomparison among plasma wake models for plasmaspheric and ionospheric conditions, Planet. Space Sci., 35, 1477–1487, 1987.

Samir, U., Israelevich, P., Wright, K. H., and Stone, N. H.: Ion temperature enhancement in the wakes of ionospheric spacecraft, J. Geophys. Res., 106, 12 963–12 968, 2001.

Séran, E.: Reconstruction of the ion plasma parameters from the current measurements: Mathematical tool, Ann. Geophys., 21, 1159–1166, 2003,
SRef-ID: 1432-0576/ag/2003-21-1159.

Singh., N., Samir, U., Wright, K. H., and Stone, N. H.: A possible explanation of the electron temperature enhancement in the wake of a satellite, J. Geophys. Res., 92, 6100–6106, 1987.

Siskind, D. E., Raitt, W. J., Banks, P. M., and Williamson, P. R.: Interactions between the orbiting space shuttle and the ionosphere, Planet. Space Sci.,32, 881-896, 1984.

Swift, J. D. and Schwar, M. J. R.: Electrical probes for plasma diagnostics, ILIFFE book ltd, London, 1970.